Neural Computing and Applications
https://doi.org/10.1007/s00521-021-05851-9

ORIGINAL ARTICLE

Map-aided and UWB-based anchor placement method in indoor localization

Hao Pan[1] · Xiaogang Qi [1] · Meili Liu [1] · Lifang Liu[2]

Received: 16 November 2020 / Accepted: 19 February 2021

Abstract
Nowadays, ultra wideband (UWB) has been popular in indoor positioning systems. Because of obstacles such as walls, doors, desks and pedestrians in the indoor area, UWB devices have to be conducted in a non-line-of-sight (NLOS) environment. The placement of nodes has significant influences on the performance of localization. In this paper, an anchor placement method for the target's trajectory based on genetic heuristic differential evolution algorithm is proposed to improve the UWB localization accuracy. To be specific, in an area with low anchor densities, a target does not have enough anchors for multilateration localization; thus, a coverage degree criterion is defined. Meanwhile, the Cramer–Rao lower bound (CRLB) is used as an evaluation metric for localization accuracy, and both of CRLB and coverage degree criterion are incorporated into the evaluation function of the differential evolution (DE) algorithm. Furthermore, instead of using the liner distance path loss model, the more practical UWB-based through-wall signal propagation model is adopted to reflect the influences of obstacles that are widespread in indoor environments. In addition, a software application is developed to visualize the indoor scenario, signal propagation status and anchor placement results. Finally, field experiments and simulations are performed, and a thorough case study confirms the effectiveness of the proposed method. The average localization error of the proposed placement scheme can be reduced by 28.2% and 12.5% compared to the random scheme and the default DE-based scheme.

Keywords Indoor localization · Ultra wideband · Differential evolution algorithm · Simulation software

1 Introduction

Nowadays, GPS-based positioning systems can provide satisfactory and reliable performance in open outdoor areas. However, many missions require localization service in caves and buildings, these environments may cause deterioration or complete prevention of the GNSS signals [11, 31], and indoor navigation systems still involve some challenges in terms of robustness and accuracy. Because of many obstacles such as walls, doors, desks and pedestrians in the indoor area, it is difficult to obtain reliable and accurate measurements. Many efforts have been made to study the indoor navigation problem from different perspectives [5, 24, 33, 39]. Most of them can be categorized into two main categories: infrastructure based and infrastructure-less.

Owing to the ubiquity of wireless networks and popularity of WiFi and Bluetooth infrastructures, infrastructure-based indoor navigation systems have attained much attention in both academia and industries. Fingerprint localization approach is usually used in indoor navigation systems, and it consists of two steps named training and positioning. Many efforts have been made to improve such steps. In the training step, the fingerprint data collecting task is a very time-consuming task in a large area or a dynamic indoor environment, and Jie et al. propose an automatic offline database construction method in a hybrid UWB/WiFi environment [13]. In the positioning step, Jin and Liu proposed a zero site-survey overhead (ZSSO) algorithm and transfer learning-based framework to enhance the system scalability [14, 21], respectively. AL-

✉ Hao Pan
hpan@stu.xidian.edu.cn

[1] School of Mathematics And Statistics, Xidian University, Xi'an, China

[2] School of Computer Sciences, Xidian University, Xi'an, China

Published online: 17 March 2021

Madani and Orujov et al. propose a fuzzy logic-based scheme to select the best localization algorithm depending upon the size of the room, and two-type fuzzy logic-based algorithms are proposed to improve the localization accuracy and navigation effectiveness [1, 22].

Range-based approach is usually used in infrastructureless indoor navigation systems, and localization is only based on information from reference nodes with known positions which named anchors. The information includes at last the range measurements and the locations of the anchors. The relatively new ultra wideband (UWB) technique is a non-carrier radio communication technology with a narrow signal in the time domain and wide bandwidth in the frequency domain. Many application scenarios require sub-meter-level positioning services, such as warehouse positioning and indoor unmanned systems. Hence, it has attracted extensive attention due to its high-ranging accuracy [3]. Emerging applications of UWB localization systems have been presented by using the product from Ubisense, BeSpoon and DecaWave.

In an indoor area, it normally divided with obstacles, walls which can affect the radio frequency (RF) waves distribution. When the direct propagation path is replaced by the reflected path, it increases the propagation time and causes randomness in the error due to the uncertainty of the reflected path. When the RF waves traverse an obstacle, the changed path direction will increase propagation distance, and the permittivity of the obstacle will reduce its propagation speed. Hence, as the ratio of NLOS measurement increases, the accuracy of the UWB localization system decreases. Therefore, optimal placement of the anchors and eliminating the NLOS effect are critical for improving the localization accuracy. Accordingly, we aim at proposing a UWB-based anchor placement framework to reduce the localization error.

In this work, a map-aided and trajectory-based indoor anchor placement method is proposed to improve the quality of the UWB-based indoor localization services. Following the step of typically node placement optimization method, in particular, the main contributions of this work are outlined as follows:

1. We establish a CRLB-based objective function for judging the quality of 3D multilateration localization. Due to that walls can affect the radio frequency (RF) waves propagation, we investigate the UWB-based signal propagation model and train the through-wall attenuation model through actual measurement data which collected by using DWM1000-based equipment. In order to represent the relationship between floor plan and movement trajectory, a graph-based indoor element representation method is introduced. Based on the above models, we use the differential evolution algorithm as the selection algorithm. The indoor area will be divided according to the movement trajectory represented by graph, and the search space is constrained in the relevant area.
2. In order to save time costs, we propose a software tool using computer-aided simulation to achieve the signal propagation measurement model and execute the node placement methods. In the process of anchor placement, the visualization function of location and propagation path blocking information between nodes can directly show the placement results, and the relevant staff can adjust the location of nodes according to the visualization results. The comparative experimental results show that our simulation tool can simulate the NLOS propagation path blocked by the concrete wall according to the indoor scene. The through-wall signal propagation model can be used more effectively in our proposed method. In addition, users can define their own scenario, node placement algorithm and localization algorithm, and the localization accuracy of the different anchor node placement can be calculated.
3. In order to explain specifically the influence of UWB nodes placement scheme on localization performance, two localization experiments, we conduct a real-world field test and performance evaluation. First of all, we use the total station and laser rangefinder to set the coordinates of the important landmarks on the ground. The comparison experiments of bad anchor placement and typical placement are conducted by using the UWB equipment. Then, we conduct the NLOS measurement experiment by setting UWB equipment on both sides of the wall, and we collect the range measurement data by changing the position of the receiving node and training the signal propagation model. Last but not least, a thorough case study is proposed by conduct four different comparison setups, and the results confirm the effectiveness of the proposed algorithm. The experimental results conclusively demonstrate the effectiveness and the improvement of our proposed method.

2 Related works

In this section, we briefly review existing works related on optimizing anchor or AP placement to improve localization and navigation accuracy.

The placement of AP affects the discrimination of the fingerprints in the radio map and has a great influence on the localization system. The optimization node placement method can be used to improve the estimate accuracy in indoor localization systems. The placement optimization

method typically relates to the following aspects: the metric of the quality of a node placement scheme, the search algorithm and the signal propagation model.

Various localization performance criteria have been proposed. The variation of RSS measurements is induced to evaluate localization performance, and researchers use it as the objective function of their AP and Beacon placement method [4, 6, 9, 27]. Zirazi proposed the concept of the geometric dilution of precision (GDOP) that is utilized as a metric of the localization performance [41]. Similarity, Sadhukhan introduced a clustering strategy-based localization performance criteria and presented an optimal n-coverage visibility beacon placement strategy [25]. These localization performance criteria are proposed in fingerprint localization scheme, and they prefer to investigate node placement method based on AP node k coverage problems. The problem that finds an optimal node placement is NP complete [23, 29]. Many researchers have dealt with similar problem using different heuristic algorithms, such as simulated annealing algorithm [6], the genetic algorithm (GA) [17, 37], particle swarm optimization (PSO) [7, 16, 20] and the differential evolution algorithm (DE) [30, 40]. However, the practicability of the node placement scheme depends on the signal propagation model. As to the wireless signal, the log distance path loss (LDPL) model was used in many studies [4, 32], which is suitable for LOS environment. The Motley–Keenan model and the ray tracing propagation model can embody the attenuation caused by obstacles, and they were used in [9, 12] and [15, 28], respectively.

In fact, for both two indoor localization method, the placement of the sensor nodes has a large impact on the localization accuracy of the target [34]. In some narrow space, the bad node placement scheme greatly reduced the localization accuracy. Recently, many researchers studied the placement method in the line-of-sight (LOS) environments. With help of the Cramer–Rao lower bound (CRLB) which is widely used as an evaluation metric for localization accuracy [8], the optimal nodes geometry has been researched by adopting the CRLB as the objective function. Wang et al. [18] proposed a search algorithm based on genetic algorithm (GA) for determining the best node placement scheme. Similar to the GDOP metric used in fingerprint localization [41], Lin et al. introduce the position dilution of precision (PDOP) as the performance metric and propose a node placement method for multilateration localization algorithm [38]. In order to reduce the search time, ant colony optimization (ACO) algorithm is used to solve the node placement problem [7]. A harmony search (HS)-based deployment algorithm is proposed to maximizing the network coverage and minimizing the network cost [2]. As for UWB localization networks, a search method for the optimal placement of the nodes based on genetic algorithm (GA) is proposed, and it aims to improve the multilateration localization accuracy in a narrow space [34].

In summary, although the existing studies have proposed various optimization methods, there still exist various challenges. As for fingerprint-based positioning system, due to its tolerance to pervasive multipath effects, it has been widely used in indoor environments. But in multilateration-based positioning systems, the distance measurements have great impact on the estimation accuracy. Thus, the objective of the anchor node placement method for fingerprint-based localization systems and multilateration-based localization system is different. Although both of two methods need to consider the obstacles between the target and the anchor, in multilateration-based node placement method, the angel and number of the LOS measurements between the target and the anchor must be considered. On the other hand, many of the above node placement methods are aimed at the entire area. In practical applications, the target will use the planned fuzzy trajectory to perform some tasks, such as fire rescue and indoor survey. For the purpose of saving energy and cost, the wireless positioning devices are placed to cover the planned trajectory. In addition, for same number of devices, trajectory-based node placement method can improve the localization accuracy.

3 Methodology

3.1 The measurement model and CRLB metric for localization

In this paper, we consider using N static time-of-arrival (TOA) anchors, whose locations are known with negligible errors, to localize a static target in the 3D space. The noisy TOA measurement t takes:

$$\hat{d}_i(\mathbf{X}) = d_i(\mathbf{X}) + n_i = \|\mathbf{A_i} - \mathbf{X}\| + n_i \tag{1}$$

where $\hat{d}_i(\mathbf{X})$ is the range measurement between anchor i and target, and $d_i(\mathbf{X})$ is the true distance. The measurement errors of n_i are assumed to be i.i.d. Gaussian noises with mean zero and variances σ_i^2, $n_i \sim N(0, \sigma_i^2)$. $\hat{\mathbf{X}}$ is denoted as the estimate of the target location of $\mathbf{X}$, and then, the estimation error covariance matrix is:

$$\Phi = E\left\{(\hat{\mathbf{X}} - \mathbf{X})(\hat{\mathbf{X}} - \mathbf{X})^{\mathbf{T}}\right\} \tag{2}$$

Hence, in order to obtain the CRLB for 3D TOA target localization, we will derive the closed-form formulas of the Fisher information matrix (FIM) in the following. It is well known that maximum likelihood estimation MLE can

achieve CRLB asymptotically. The logarithmic likelihood function with respect to $\mathbf{X}$ is given by:

$$\ln f\left(\hat{d}_i \mid \mathbf{X}\right) = \ln\left(\sqrt{2\pi}\sigma_i\right) + \frac{\left[\hat{d}_i - d_i(x)\right]^2}{2\sigma_i^2} \tag{3}$$

The FIM for 3D TOA target localization is defined as:

$$\mathbf{F} = E\left\{\left[\frac{\partial}{\partial \mathbf{X}}\ln f\left(\hat{d}_i \mid \mathbf{X}\right)\right]\left[\frac{\partial}{\partial \mathbf{X}}\ln f\left(\hat{d}_i \mid \mathbf{X}\right)\right]^{\mathbf{T}}\right\} \tag{4}$$

According to the logarithmic likelihood function:

$$\frac{\partial}{\partial \mathbf{X}}\ln f\left(\hat{d}_i \mid \mathbf{X}\right) = \sigma_i^{-2}\left[\hat{d}_i - d_i(\mathbf{X})\right]\frac{\partial}{\partial \mathbf{X}}d_i(\mathbf{X}) \tag{5}$$

Using Eqs. (3) and (4), the FIM can be expressed as:

$$\mathbf{F} = \left[\frac{\partial}{\partial \mathbf{X}}d_i(\mathbf{X})\right]C^{-1}\left[\frac{\partial}{\partial \mathbf{X}}d_i(\mathbf{X})\right]^{\top} \tag{6}$$

where C^{-1} is the sensor measurement covariance matrix.

The CRLB for TOA-based localization is given by the following:

$$\mathbf{F}^{-1} = \left[\mathbf{G}\mathbf{C}^{-1}\mathbf{G}^{\top}\right]^{-1} \tag{7}$$

where $\mathbf{G} = [\mathbf{g_1}, \mathbf{g_2}, \quad, \mathbf{g_n}]$, and $\mathbf{g_i}$ can obtain

$$\begin{aligned}\mathbf{g_i} &= \frac{\partial d_i(\mathbf{T})}{\partial \mathbf{T}} = \left[\frac{\partial d_i(\mathbf{T})}{\partial x_T}, \frac{\partial d_i(\mathbf{T})}{\partial y_T}, \frac{\partial d_i(\mathbf{T})}{\partial z_T}\right]^T \\ &= 2 \cdot \begin{bmatrix} \frac{x - x_i}{\sqrt{(x-x_i)^2+(y-y_i)^2+(z-z_i)^2}} \\ \frac{y - y_i}{\sqrt{(x-x_i)^2+(y-y_i)^2+(z-z_i)^2}} \\ \frac{z - z_i}{\sqrt{(x-x_i)^2+(y-y_i)^2+(z-z_i)^2}} \end{bmatrix}\end{aligned} \tag{8}$$

An example is shown in Fig. 1. In 3D scene, we further introduce another auxiliary phase variable vector in terms of the elevation angle ϕ_i and azimuth angle ψ_i commonly used in vector representing [19], and then, we get:

$$\mathbf{g_i} = \begin{bmatrix} 2\cos\phi_i\cos\psi_i \\ 2\cos\phi_i\sin\psi_i \\ 2\sin\phi_i \end{bmatrix} \tag{9}$$

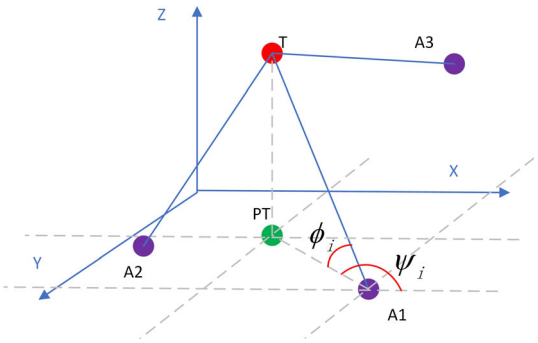

Fig. 1 The illustration of true target localization using TOA

This criterion results in minimizing the average variance of the estimates of the regression coefficients. According to Eqs. (7) and (9), the $Tr(\mathbf{F})$ can be expressed as:

$$\begin{aligned}Tr(\mathbf{F}) = 4\sigma_i^{-2}\Bigg(&\sum_{i=1}^{M}\cos^2\phi_i\cos^2\psi_i + \sum_{i=1}^{M}\cos^2\phi_i\sin^2\psi_i \\ &+ \sum_{i=1}^{M}\sin^2\phi_i\Bigg)\end{aligned} \tag{10}$$

The CRLB refers to the theoretical lower limit of the unbiased estimator, and it has been a commonly applied evaluation standard for target localization accuracy. It can be adopted to evaluate the performance of different node placement schemes. From the above formulations, the optimal nodes placement does not depend on the distances between the target and anchors. It only depends on the directions from the target to anchors, which will be well considered in the proposed algorithm.

3.2 Signal propagation model

As the radio frequency (RF) waves propagate through the air, their speed is approximately at the speed of light. RF waves traverse a wall, the permittivity of the wall causes the wave to change direction and reduce its propagation speed. The propagation speed of an RF wave in a wall can be calculated as [11]:

$$v_{\mathrm{rf}} = \frac{c}{\sqrt{\varepsilon_{\mathrm{r}}}} \tag{11}$$

where ε_{r} is the real relative permittivity of an obstacle, and c is the speed of light through the air. From Eq. (11), it can be easily obtained that the speed of wave decreases in a wall. Hence, it makes the signal longer to propagate the wall in comparison with air consequently increasing the ToF measurement. Figure 2 shows the signal propagation model that calculates the ToF from the transmitter to the receiver through a wall. The ToF from an anchor in location A to a tag in location D is given by:

$$t_{\mathrm{AD}} = t_{\mathrm{AB}} + t_{\mathrm{BC}} + t_{\mathrm{CD}} = \frac{1}{c}\left(d_{\mathrm{AB}} + d_{\mathrm{BC}} + d_{\mathrm{CD}}\right) \tag{12}$$

where the t is the ToF for the different propagation path, and d denotes the distance.

According to Eq. (12), the ToF can be rewritten as:

$$t_{\mathrm{AD}} = \frac{1}{c}\left(d_{\mathrm{AB}} + d_{\mathrm{BC}}\sqrt{\varepsilon_{\mathrm{r}}} + d_{\mathrm{CD}}\right) \tag{13}$$

where d_{BC} is the distance of the propagation path that traversed in the wall, and w denotes the wall's thickness shown in. It can be expressed as $d_{\mathrm{BC}} = \frac{w}{\cos\alpha_t}$, and the

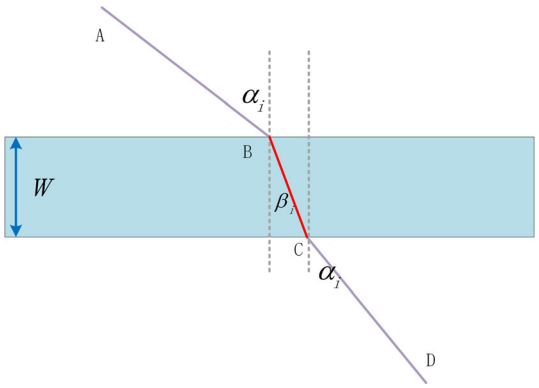

Fig. 2 Through-wall distance measurement

transmission angle α_t is related to the incidence angle β_t by Snell's law:

$$\lambda_1 \sin \beta_t = \lambda_2 \sin \alpha_t \tag{14}$$

where λ_1 and λ_2 are the refractive indexes of air and the wall, respectively. Hence, $\sin \alpha_t = \frac{\sin \beta_t}{\sqrt{\varepsilon_r}}$, and then, combined with Eqs. (14) and (13), the NLOS range becomes:

$$d_{\mathrm{AD}} = d_{\mathrm{AB}} + \frac{w\sqrt{\varepsilon_r}}{\cos\left(\arcsin\left(\frac{\sin \beta_t}{\sqrt{\varepsilon_r}}\right)\right)} + d_{\mathrm{CD}} \tag{15}$$

3.3 The metric for coverage

The metric for evaluating RF signal coverage is introduced in this section. In range-based multilateration localization method, the basic condition for the algorithm is that a target has enough anchors for multilateration. An indoor area satisfies n-degree if and only if the target at any reference location in this area is able to communication with anchors above a threshold from at least n. The placement of anchors is denoted as $\mathbf{P}$, the coverage ratio as the percentage of the reference points in an area which satisfy n-degree coverage:

$$\tau_n(\mathbf{P}, n) = \frac{\sum_{i=1}^{m} \mathrm{Cov}(\mathbf{P}, n, i)}{m} \tag{16}$$

where m is the number of reference points, and

$$Cov(\mathbf{P}, n, i) = \begin{cases} 1, & \text{satisfies n-degree coverage} \\ 0, & \text{otherwise} \end{cases} \tag{17}$$

4 Algorithm

4.1 Indoor map and trajectory representation

The current indoor positioning techniques often regard the indoor environment as grid or Cartesian space, given the floor map. However, giving the 2D positions is not always beneficial. Normally, due to the user's activity in small space, moving distance and time spending for stay are much shorter indoor than outdoor, and a positioning system may make the target's trajectory including outlier and missing position. A less rigid representation is called semantic positions, and it can be better than 2D positions. Users will understand the inferred pattern *Toilet* $\rightarrow$ *Hallway* better rather than $(1, 5) \rightarrow (4, 3)$. The challenge exists in the lack of standard representation rules to define all the elements in an indoor map.

In this work, the regionalized representation of the trajectory is the prerequisite for studying the area coverage problem. If a set of discrete coordinates is used to represent the trajectory, the anchor nodes cannot be arranged according to the wall distribution.

Figure 3 once again illustrates the importance of the anchor node placement scheme. Figure 3a shows an empty environment, the path is covered by a rectangle, and the anchor placement scheme adopts uniform angular arrays placement method [35], which can obtain enough range measurement from different directions in the process of target movement. However, considering the indoor scenario, the target cannot obtain enough LOS range measurement in the process of movement. As shown in Fig. 3b, the target obtains a large number of NLOS range measurements in the central corridor, and it may lead to serious localization errors. Under the same number of anchors, if a sufficient number of anchor nodes are placed in the region (the open area divided by concrete walls) which the target passes, as shown in Fig. 3c, the target can obtain sufficient LOS range measurements. Although there is interference from NLOS ranging caused by anchor nodes in other areas, the interference caused by NLOS ranging to position

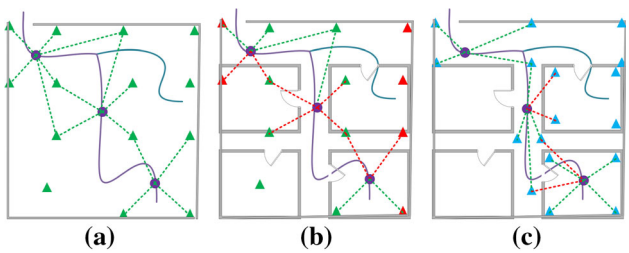

Fig. 3 Sensor nodes placement schemes. **a** Nodes placement scheme without considering the indoor scenario. **b** Nodes placement scheme in an indoor scenario. **c** Nodes placement scheme considering the indoor scenario

Table 1 Elements in formulated indoor scenario

Type	Area	Element	Description
Node	Intersection	Turing point	Conjunction between corridors
	Door	Doo	Conjunction between corridor and open area
	Open area	Room	Relatively empty space
Way	Corridor	Corridor	Long and narrow space

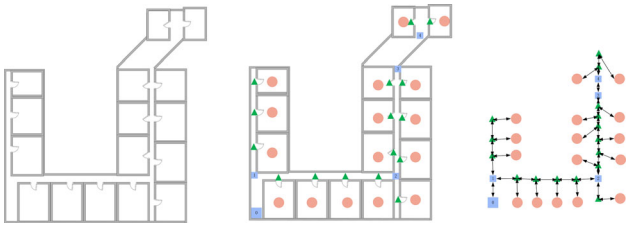

Fig. 4 The schematic diagram of area element representation

estimation can be reduced through appropriate constraints. Particularly in the corridor area, this placement scheme can effectively increase the number of LOS range measurements.

These markers allow us to set the rules by labeling the nodes as intersections and open areas, and the ways as corridors and walls. All the basic elements in an indoor map are shown in Table 1. According to the map structure, we divide the indoor environment into three main types of area states: open areas, intersections and corridors. The schematic diagram of area state representation on the map is presented in Fig. 4.

4.2 The CRLB-based differential evolution algorithm

As searcher method, the differential evolution algorithm is originally proposed to solve the continuous optimization problem. In this work, we adopt CRLB to evaluate the individual, and the CRLB-based differential evolution algorithm is introduced to search the optimal node placement. The node placement algorithm is described in Algorithm 1, and the specific operation is illustrated as follows.

Algorithm 1 The CRLB based differential evolution algorithm

Require:
$i-th$ fixed anchor information, $\mathbf{A_i}$;
Trajectory represented by graph, $\mathbf{G_t}$;
Grid width, D_p;
Scaling factor, F;
Coverage ratio, R_c;
Population number of each open area, Pn;
Evaluation vaule, $CRLB + \sigma$;
Max iterative, T_{max};
Ensure:
The best individual list for each area, $\mathbf{I}_{best} = \{\}$;
for Each area $\mathbf{G_i}$ in the trajectory $\mathbf{G}$ **do**
  $t = 1$
  while $t \leq T_{max}$ **do**
    $t = t + 1$
    $e_P = Evaluation()$
    if $e_P \leq CRLB + \sigma$ **then**
      Break;
    end if
    for I_i In P_{G_i} **do**
      /*Operation for the individual I_i
      for G_i In I_i **do**
        /*Operation for the genes in individual I_i */
        $GM_i = Mutation(G_i, F, D_p)$;
        $C_i = Crossover(G_i, GM_{i,j}, P_c)$;
      end for
      $\varepsilon_L(GM_i) = IndividualEvaluation(GM_i)$;
      $\varepsilon_L(C_i) = IndividualEvaluation(C_i)$;
      if $\varepsilon_L(GM_i) \leq \varepsilon_L(C_i)$ **then**
        $I_i = GM_i$;
      end if
    end for
  end while
  $I_{best,i} = Selection()$
  $I_{best} = Append(I_{best,i})$
end for

(1) Initial population.

The initial step is aim to encode the solution as the gene. The population is initialized to represent the search space. According to the graph representation method, the initial population is distributed in the area passed by the trajectory, it is composed of multiple individuals, and each individual is a candidate solution and composed of multiple genes. The initial population should cover the whole trajectory. While the population size increases, the probability of obtaining the global optimal solution will increase. In this step, the information of the anchors is used as gene codes, and the gene sequence can be expressed as:

$$\mathbf{GS} = [pos, ld, fx, r] \tag{18}$$

where *pos* denote the coordinates of the anchor, it can be expressed as $pos = [x, y, z]^{\mathrm{T}}$, r denotes the measurement range of the anchor, fx denotes whether is a preexisting anchor, and ld denotes the description of the location, which is introduced in the above section. If the fx value is 0, the coordinates of anchors are generated randomly. The anchors' fx with a value of 1 are specified by the user as initial parameters and are fixed during operation. It is noticeable that the fixed anchors can reduce the search time.

In this work, the location service should cover the whole trajectory. The trajectory is represented as the graph which is consisted of areas. Different from covering the entire area, we initialize the population of the area where the trajectory includes. We generate individuals in these areas. Let $\mathbf{P} = [\mathbf{P_1}, \mathbf{P}_2, \ldots, \mathbf{P_w}]$ denote the population and $\mathbf{P_w}$ denote the population in the w-th area. In an area, population consist of many individuals, $\mathbf{P}_w = [\mathbf{I_1}, \mathbf{I_2}, \cdots, \mathbf{I_M}]$, where $\mathbf{I_j} = [\mathbf{G_1}, \mathbf{G_2}, \cdots, \mathbf{G_n}]$ denotes the j-th individual, n is the number of genes, and M is the number of individuals. As a result, $M \times n \times w$ anchors are generated to form the initial population, and each individual is an anchor placement.

(2) Individual evaluation.

In this work, CRLB is used to represent the minimum localization error of a location. The average localization error and the coverage ratio are used to evaluate the individuals. The objective of the algorithm is that the individual has lower average localization error under the coverage requirement. The evaluation value of each individual is:

$$f_E(\mathbf{P_w}) = \begin{cases} \dfrac{1}{\varepsilon_L(\mathbf{P_w})} & \tau_n(\mathbf{P}, n) \geq R_c \\ 0 & \text{otherwise} \end{cases} \tag{19}$$

where $\mathbf{I_j}$ is the j-th individual, R_c is the coverage ratio threshold, and $\varepsilon_L(\mathbf{P_w})$ is the average localization error at all locations in area w, which is used CRLB as the localization performance. It is denoted as:

$$\varepsilon_L(\mathbf{P_w}) = \frac{\sum_{j=1}^{p} Tr\left(\mathbf{F}^{-1}(\mathbf{x}_j)\right)}{pn} \tag{20}$$

where pn is the number of test locations, and $\mathbf{x}_j$ is the coordinate of the j-th location in area w.

(3) Mutation.

The objective of mutation operation is creating a new individual, and the basic principle is to add a difference vector to a base vector. For example, the mutation operation will produce a corresponding donor vector for each individual. The deviation vector can also be generated in five methods, usually expressed in the form of *DE/x/y/z*, including *DE/rand/1/bin*, *DE/best/1/bin*, $DE/rand-to-best/1/bin$, *DE/best-/2/bin*, *DE/rand/2/bin*. x indicates whether the current donor vector is random or best, y indicates the number of difference vectors, and z indicates the operation method of the crossover procedure, such as binomial crossover operation.

In this problem, the objective of mutation operation is changing the x, y and z value of each gene individuals I, denoted as $\mathbf{G}_i$, and produces the donor vector $\mathbf{M}_i$ of individual i. The mutation operation formula of x, y and z value in $\mathbf{G}_i$ can be written as:

$$\begin{cases} x_{GMV_{ij}} = x_{G_{ij}} + \rho \times F \times D_p & j \in [1, n] \\ y_{GMV_{ij}} = y_{G_{ij}} + \rho \times F \times D_p & j \in [1, n] \\ z_{GMV_{ij}} = z_{G_{ij}} + \rho \times F \times D_p & j \in [1, n] \end{cases} \tag{21}$$

where $\mathbf{G}_{i,j}$ are the j-th gene of the individual i, $x_{MV_{ij}}$, $y_{MV_{ij}}$. $\mathbf{GM}_{i,j}$ denotes the j-th gene of the mutant individual $\mathbf{M}_i$. $z_{MV_{ij}}$ are the x, y and z values of the mutant gene $\mathbf{GM}_{i,j}$, $x_{G_{ij}}$, $y_{G_{ij}}$ and $z_{G_{ij}}$ are the x, y and z values of gene $\mathbf{G}_{i,j}$, ρ is an integer randomly chosen from the range $[-1, 1]$, *and* F is an integer and controls differential variation. D_p is the grid distance to get placement points by dividing the area. After mutation operation, the genes of the individual should be ensured in search space.

(4) Crossover.

In this step, the individual $\mathbf{C}_i$ can be obtained by using the binomial crossover method that cross genes of $\mathbf{I}_i$ and $\mathbf{GM}_{i,j}$ after mutation operation. where P_c denotes the crossover probability.

However, after crossover operation, it may result in duplicate genes in the individual. Simple distance limitation of two genes is not suitable especially in range-based localization, which the indoor environments exist many obstacles. In this work, the individuals are placed in each area which is included in the trajectory. In same area, if the gene distance measurements from other genes are small than threshold D_t, it will randomly generate its x, y and z values.

(5) Selection.

The differential evolution algorithm selects individuals from the experimental population $\mathbf{P_w}$ as individuals in the next generation population according to the greedy criterion.

5 Simulation tools and experiments

In order to validate the effectiveness of the proposed method, we conduct the compared node placement experiment. Also, we verify the bias and ranging models experimentally. After that, we introduce our simulation tool based on Python3 and PYQT5. The tool supports the scenario generation and synthetic generation of signals based on UWB through-wall signal propagation model. We conduct a small trial to validate that the signal propagation through the wall can be detected in our tool, and it is important for the signal propagation model. At last, to determine the improvement in location accuracy, we conduct a case study with four setups.

5.1 Node placement experiment

In order to explain specifically the influence of UWB nodes placement on localization performance, two localization experiments were carried out. In this section, the experiments include a typical placement and a bad placement scheme. The equipment (Fig. 5a) used in experiments is an ultra wideband (UWB) transceiver module based on Decawave's DW1000 design. It integrates antenna, RF circuit, power management and clock circuit. It supports two-way ranging or TDOA measurement, and data rates are up to 6.8 Mbps. Table 1 shows the key performance parameters of the equipment.

The experiment area is 20 m long and 10 m wide (shown in Fig. 6), and two experiments are conducted. In the first experiment, the anchors are placed in the corners (shown in Fig. 7a). In another experiment, the anchors are placed in a bad placement (shown in Fig. 7b). The coordinates of all anchors and locations are measured by total station (shown in Fig. 5b). The z-axis coordinates of four anchor nodes in the typical experiment are set to 0.3 m, 1.7 m, 1.7 m and 0.24 m, but in bad nodes placement experiment, the z-axis coordinates of anchors are set to 1.3 m, 1.7 m, 1.7 m and 1.24 m. The z-axis coordinates of these target locations are all set to 0.3 m. Each location was repeatedly measured fifty times.

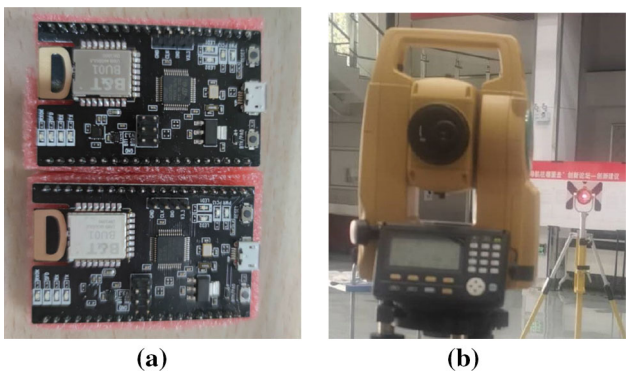

Fig. 5 The external view of the equipment in our experiments. **a** UWB equipment. **b** Total station

Fig. 6 The experiment environment

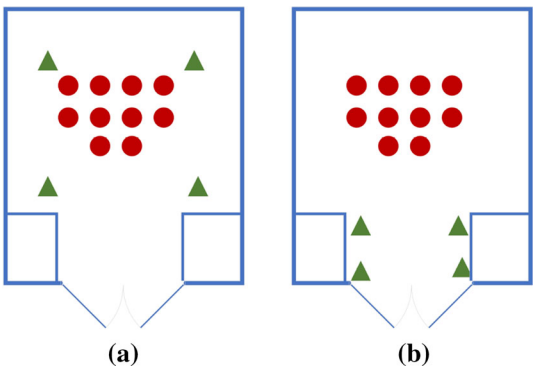

Fig. 7 Floor plan of experiment area. **a** Typical nodes placement experiment. **b** Bad nodes placement experiment

In the typical nodes placement experiment, the anchors are placed around the experiment area. The coordinates of reference are listed in Table 2

As shown in Table 3, the average localization error in x-axis, y-axis and z-axis was 0.063 m, 0.109 m and 0.225 m, respectively. The standard deviation was 0.031 m, 0.087 m and 0.163 m. In the experiment of typical node placement method, the average localization error in z-axis is little larger than x-axis and y-axis. In addition, the standard deviation has similar result.

In the bad nodes placement experiment, the anchors are placed around the experiment area, as shown in Fig. 7b. The coordinates of reference are listed in Table 4. The results of the bad node placement experiment are shown in

Table 2 Anchors location in typical nodes placement experiment

Anchors id	Coordinates
A1	0, 0, 0.3
A2	6.5, 0, 1.7
A3	0, 9.5, 0.24
A4	6.5, 9.5, 1.7

Table 3 Elements in formulated indoor scenario

True	Estimate	δx/m	δy/m	δz/m
1.5, 1.3, 0.3	1.394, 1.327, 0.262	0.106	0.027	0.038
1.5, 3.2, 0.3	1.405, 3.042, 0.227	0.095	0.158	0.073
1.5, 5.1, 0.3	1.570, 5.116, 0.187	0.071	0.016	0.113
2.2, 1.3, 0.3	2.122, 1.284, 0.375	0.078	0.016	0.075
2.2, 3.2, 0.3	2.160, 2.919, 0.484	0.040	0.281	0.184
2.2, 5.1, 0.3	2.195, 4.959, 0.376	0.005	0.141	0.076
2.2, 7.0, 0.3	2.220, 6.981, 0.511	0.020	0.019	0.211
2.9, 1.3, 0.3	2.963, 1.170, 0.785	0.063	0.130	0.485
2.9, 3.2, 0.3	2.988, 3.270, 0.527	0.088	0.070	0.227
2.9, 5.1, 0.3	2.826, 4.990, -0.087	0.074	0.109	0.387
2.9, 7.0, 0.3	2.824, 6.969, 0.209	0.076	0.031	0.091
3.6, 1.3, 0.3	3.651, 1.071, 0.714	0.051	0.229	0.414
3.6, 3.2, 0.3	3.578, 3.114, 0.043	0.022	0.086	0.257
3.6, 5.1, 0.3	3.521, 4.895, 0.249	0.079	0.205	0.513

Table 5 Elements in formulated indoor scenario

True	Estimate	δx/m	δy/m	δz/m
1.5, 1.3, 0.3	0.937, 1.277, 2.799	0.563	0.030	2.499
1.5, 3.2, 0.3	1.002, 3.098, 2.498	0.499	0.102	2.197
1.5, 5.1, 0.3	1.420, 5.002, 0.620	0.080	0.098	0.320
2.2, 1.3, 0.3	2.428, 1.170, − 0.789	0.228	0.130	1.089
2.2, 3.2, 0.3	2.072, 3.187, 0.879	0.128	0.030	0.579
2.2, 5.1, 0.3	2.078, 5.024, 0.799	0.122	0.076	0.499
2.2, 7.0, 0.3	2.607, 6.854, − 1.578	0.407	0.146	1.879
2.9, 1.3, 0.3	3.030, 1.278, − 0.305	0.130	0.022	0.605
2.9, 3.2, 0.3	2.733, 3.085, 1.038	0.167	0.115	0.738
2.9, 5.1, 0.3	3.252, 5.002, − 1.292	0.352	0.098	1.592
2.9, 7.0, 0.3	3.226, 7.012, 0.458	0.326	0.012	1.499
3.6, 1.3, 0.3	3.553, 1.220, 0.519	0.047	0.080	0.219
3.6, 3.2, 0.3	3.697, 3.187, − 0.115	0.097	0.013	0.415
3.6, 5.1, 0.3	3.348, 5.061, 1.429	0.252	0.039	1.290

Table 5, the mean error in x-axis, y-axis and z-axis is 0.243 m, 0.071 m and 1.101 m, respectively, and the standard deviation is 0.157 m, 0.044 m and 0.711 m along x-axis, y-axis and z-axis, respectively.

In the case of node bad placement, the localization error in z-axis is much larger than x-axis and y-axis, and the standard deviation expressed that the fluctuation of localization error in z-axis is severer than x-axis and y-axis.

In addition, the localization error of the bad node placement experiment is much larger than the typical experiment.

The localization results of the two node placement schemes are shown in Fig. 8, the blue dot indicates the true location of the target, and the red fork indicates the estimated location. Figure 8a, b shows the results of typical node placement scheme and bad node placement scheme, respectively. In the same environment, it is obvious that the performance of any particular localization algorithm is highly related to the relative anchor–target geometry.

5.2 Through-wall experiment

To verify the bias and distance measurement models experimentally, we conducted a number of measurements using UWB equipment, which are equipped with DW1000

Table 4 Anchors location in typical nodes placement experiment

Anchors id	Coordinates
A1	1.5, 10.5, 1.7
A2	5.0, 10.5, 0.3
A3	5.0, 13.8, 1.7
A4	1.5, 13.8, 0.24

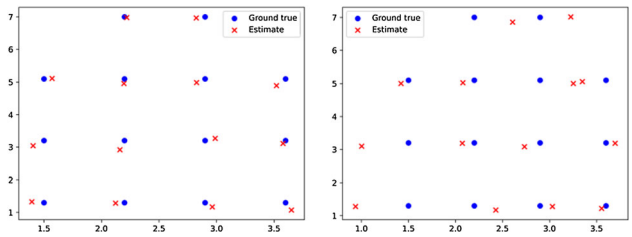

Fig. 8 Localization results of two experiments: **a** Typical nodes placement experiment. **b** Bad nodes placement experiment

UWB radios. The experiment area is 15 m long and 10 m wide, including a room and a corridor, and three types of concrete walls are selected to conduct the through-wall tests. For each target location, 100 measurements are taken; as the result, the NLOS distance is calculated as the average of these measurements.

In order to illustrate the experimental procedure, we introduce the setup for one of the experiments in detail. Same as the simulation, the anchor is fixed in an office room. The true distance is the Euclidean distance between the tag and the anchor. For each experiment, one tag and one anchor were used. A target and an anchor are distributed on both sides of the wall. We use square floor tiles as axes, and each floor tile is 50cm in length and width. The anchor is fixed at (0, 0), in the setup 1, the target initial location is (0, 2), and during the experiment, the target moves in a straight line to the location (0, 7), which is in 50-cm increments. In the setup 2, the target initial location is (2, 2), and the terminal location is (7, 7). We collect 50 distance measurements at each location. This experiment environment is shown in Fig. 10, and the thickness of the wall is 20 cm.

(a) (b)

Fig. 9 Through-wall experiment: an anchor fixed in a room (left), a target placed in a corridor outside the room (right)

In the setup 1, the angle from the target to the anchor always is 0. In the setup 2, the angel from the target to the angle always is 45. For each location along the path, we collect the true distance and measured NLOS distance. The measurements obtained from this experiment are shown in Fig. 10, and the simulated NLOS measurements line is generated by adding the bias calculated with the signal propagation model. It is obvious that the simulated and measured through-wall distances are very similar. Small

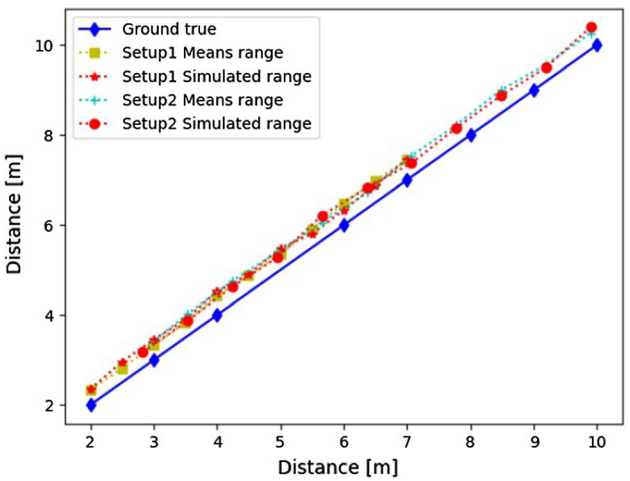

Fig. 10 Compared experiments that measured and simulated NLOS distances between the anchor and the tag for a wall with a thickness of 20 cm

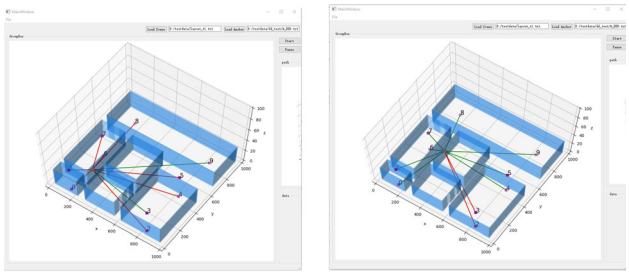

(a) (b)

Fig. 11 Measurements are generated randomly

differences can be caused by ranging noise, which is only present in the distances measured experimentally.

5.3 Measurement simulation experiment

5.3.1 Blockage detection trial

Generally, when conducting simulation experiments on indoor positioning algorithms, NLOS range measurements will be randomly generated. As UWB ranging performs in a round-robin scheme, for each anchor the ranging measurement rate is 10 Hz which is relatively low. The noise in the UWB ranging measurement is a Gaussian random noise, which is zero mean with the same variance. As shown in Fig. 14, the yellow star is the target, and the 8 purple nodes are the anchors. In Fig. 11a, the number of NLOS distance measurements is similar to the ground truth, but the specific NLOS link is incorrect. For example, the signal propagations between target and anchor1 and anchor2 are under LOS environment. However, in Fig. 11b, the number of NLOS distance measurements is incorrect. Actually, from the scenario and the position of the anchor nodes in the figure, it is easy to find that the location accuracy of the lower area is theoretically better than that of the upper area due to more anchor nodes. In the random scheme, the relationship between positioning accuracy and area cannot be reflected.

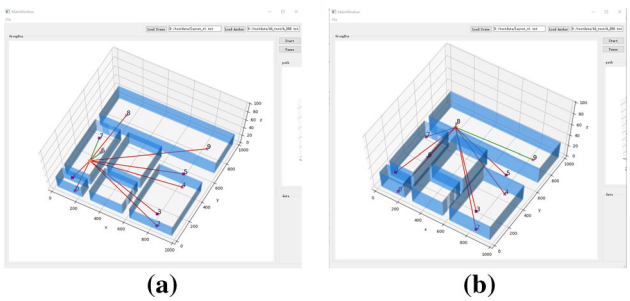

(a) (b)

Fig. 12 Measurements are generated with blockage detection algorithm

In an indoor scenario, signal propagation paths may be blocked by obstacles with a high probability. In order to simulate the distant measurements by through-wall signal propagation model, we need to detect whether there are obstacles on the path of signal propagation. An example is shown in Fig. 12a, where the purple node and yellow star represent the anchor and the target, respectively. The red line represents the topology that there are obstacles between the target and the RP, and the green line represents topology if it is not blocked by an obstacle. There are only 2 LOS measurements from node Nos. 7 and 6, respectively. The NLOS measurement between the target and the No. 1 node is blocked by 2 walls, and the distance measurement is not accuracy comparing to true distance.

In our tool, we not only need to obtain whether there are obstacles between the target and the anchors, but also visualize the obstacle, target, anchors and topology information. Throughout the tool, the signal propagation which is under NLOS environment can be visualized. As shown in Fig. 12a, b, the situation of signal generation is the same as in reality. Comparing Figs. 11 and 12, it is easy to identify the practicality of two signal propagation models.

5.3.2 Location errors for the proposed measurement model

In this experiment, we set a grid to evenly partition the area into many small square grids, and the indoor scenario is shown in Fig. 13. The center of each grid is regarded as a target. We adopt 2SWLS localization algorithm to estimate the position of each target. Based on this grid partition, the root-mean-square error (RMSE) for each grid is employed as the performance metric. Three setups are used for the comparison; as the setup 1, the NLOS measurements are generated randomly. In setup 2, NLOS measurements will be generated if there is at least one obstacle between the target and the anchor, which is illustrated in the above trial. The measurements are generated by signal propagation model coupled with the randomness of the residuals. In setup 3, true distance measurements are used, which are collected in real environment.

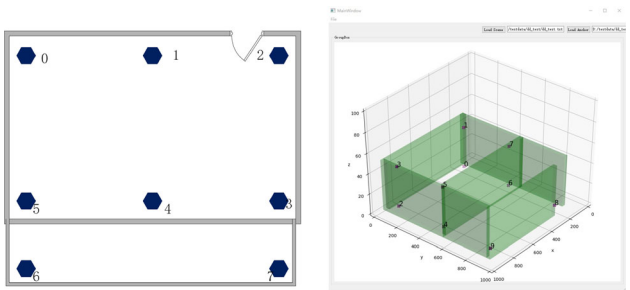

Fig. 13 The scenario and nodes placement

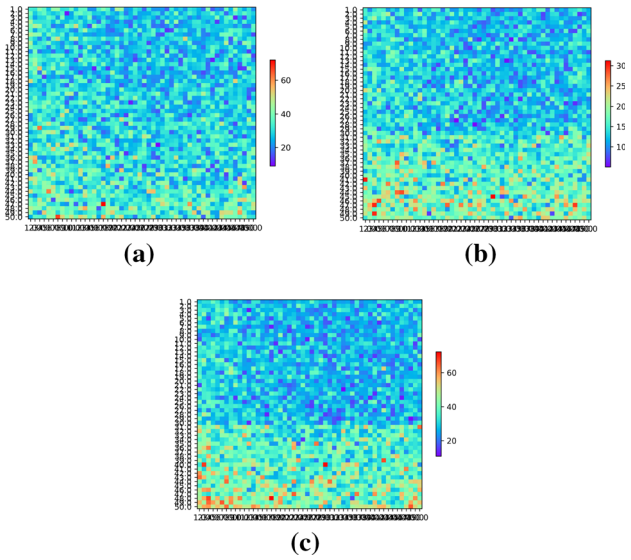

Fig. 14 The heatmap of localization errors

The results of three setups are shown in Fig. 14. From the results as shown in Fig. 14a, we can see that the absolute errors in the center area approach 0.1 m. The estimating error around the corner is slightly larger than the central area. The estimating error of the corners of the area is much larger than that of other areas. From Fig. 12, there are a number of NLOS propagations that nodes 0–5 are blocked by a wall in the upper area. As explained before, the random scheme of the measurement model is failing to simulate actual distance measurements. As shown in Fig. 14b, c, although the variance of the estimated error is not as large as in the real environment, its basic trend is the same; that is, the error increases significantly in areas with more NLOS propagation.

5.4 Case study

In order to demonstrate the effectiveness of the proposed nodes placement method, we conduct the experiment in

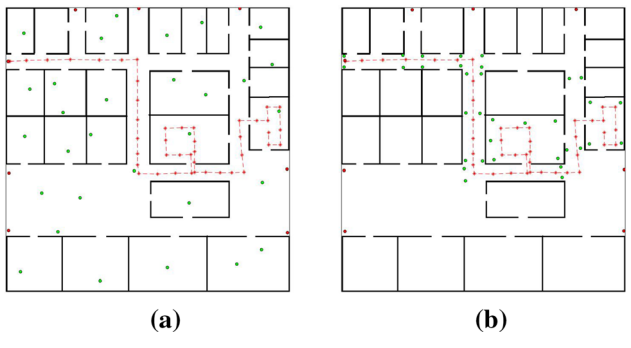

Fig. 15 Experiment environment. The green point indicates the anchor placement points, the red point indicates the fixed anchors, and the red dashed line indicates the trajectory

three setups, which is evaluated by the localization errors of the test location. The environment and trajectory are shown in Fig. 15. Compared with fingerprint localization method, UWB-based multilateral localization method needs high-accuracy range measurement. However, the range measurement error under LOS is different from that under NLOS. In this work, by using the anchor node placement algorithm, we can provide sufficient LOS measurements in each region. In addition, multilateral positioning is also affected by node geometry between target and anchors, especially in a long and narrow indoor environment. Combined with these two reasons, the environment we tested needs to include a long and narrow region and different rooms that cause non-line-of-sight interference. Although the test environment is not completely in line with the Microsoft Indoor Localization Competition, there are also some studies on the localization problem in the long and narrow environment.

There are 8 anchors placed around the area as the initial parameters for fixed anchor and represented by red point. The trajectory is represented by dashed line. The anchors locations generated by different node placement schemes are represented by green point, and the number of generated anchors is set about 30–35. In setup 1 and setup 2, the anchors are placed in the whole area, but in setup 1, we use the random scheme; in setup 2, DE-based optimal nodes placement method are used. In setup 3, the anchors are placed by our proposed method. To make the comparison, the anchor nodes are placed manually in setup 4. We apply a grid to evenly partition the area into many small square grids, each grid as the test location. Based on the grid partition, the root-mean-square error (RMSE) for each grid is employed as the performance metric which is computed using the average of 20 trials. In order to reduce the influence of other non-line-of-sight measurements on location estimation, we use QP-based localization algorithm[36], which its constraints can effectively use LOS measurements.

In order to show the test location with accuracy errors technique intuitively, the results are grouped into two parts

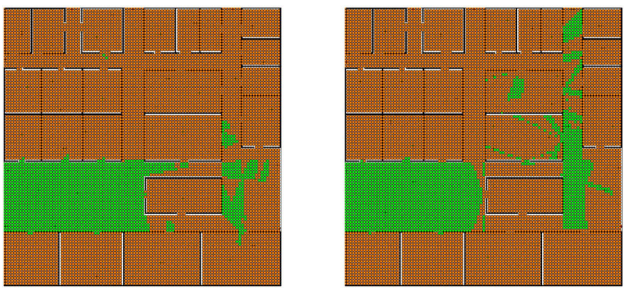

Fig. 16 Localization error of different node placement schemes which focus on the whole area. **a** Random scheme. **b** DE-based node placement scheme

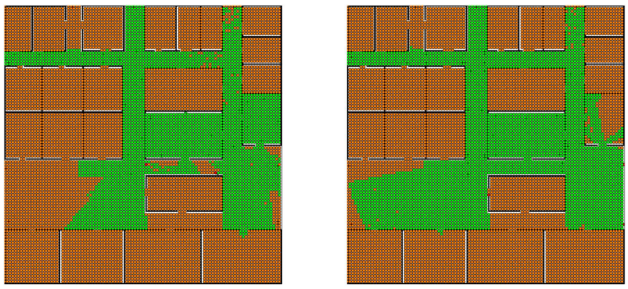

Fig. 17 Localization error of different node placement schemes which focus on the trajectory. **a** Placed manually. **b** Proposed method

by green and orange points, which represent the average accuracy less than 0.5, more than 0.5 m, respectively. In other words, the localization accuracy in green area is suitable for some task, which needs to obtain the precise location. Figure 16 shows the localization accuracy results for the node placement method which aim at the whole area. It can be seen that they have similar error distribution. Figure 17 shows the results for trajectory-based methods.

As can be seen in Fig. 17a, the average localization error around the trajectory of the proposed algorithm is less than the random method and DE-based node placement scheme. But for the whole area, these four schemes have similar accuracy. The results of our proposed method are very close to the manual method (shown in Fig. 17b), and it verifies the effectiveness of using proposed method to improve the localization accuracy. Table 6 presents a comparison of default DE scheme, random scheme, manual scheme and our proposed node placement method in terms of average error, maximum error, minimum error and the % of areas for the three groups of location errors. Except in a manual scheme, our method is leading to average and maximum errors of 0.56 and 0.88, respectively.

We removed the anchors and recalculated the average localization error to find the relationship between the localization error and anchor density. The results show that the average localization error is increasing as the density of anchors decreases (shown in Fig. 18).

We have evaluated the navigated paths using a navigation efficiency index (NEI). In this case, we evaluate the navigation result which the anchors are placed by these four different placement schemes. The results are given in Fig. 19 The measured NEI score shows that the proposed scheme can improve the navigation service and it can approach the performance of manual placement scheme in the tested indoor navigation scenarios.

The results of other authors in comparison with the current work are summarized in Table 7. Note that it is impossible to reproduce the real-life experimental conditions reported in other articles due to the very different test

Table 6 Localization error of different node placement schemes

Item(m)	Random	DE	Manual	Proposed
Average error	0.78	0.64	0.48	0.56
Maximum error	1.57	1.23	0.74	0.88
% of localizations with 0–0.5 accuracy	15	32	82	76
% of localizations with 0.5–1.0 accuracy	81	65	18	24

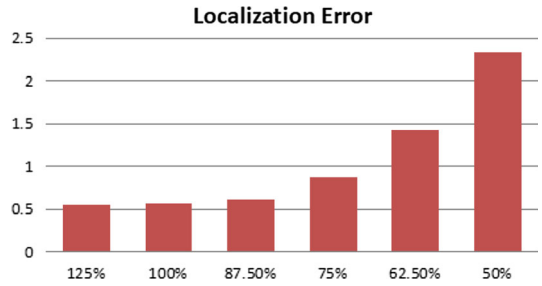

Fig. 18 Average error versus anchor density

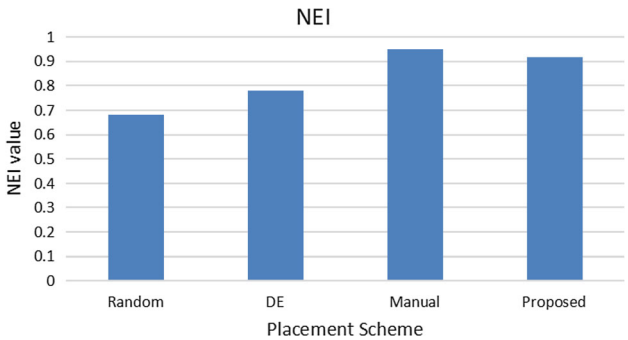

Fig. 19 Mean navigation efficiency index (NEI) versus four node placements

environments and equipment (sensing techniques) used in the respective works.

6 Conclusion

In this work, a map-aided and trajectory-based node placement method is proposed, which combines the CRLB evaluation and DE algorithm. To be specific, coverage degree, indoor scenario, through-wall signal propagation model and localization accuracy evaluation will be fully considered. In addition, a simulation tool is developed, and the experiments are carried out to verify the effectiveness of the measurement model and the tool. Finally, we conduct a positioning experiment, compared to three setups, the proposed algorithm terms of both localization accuracy and stability. Thus, the map-aided and trajectory-based node placement scheme is more suitable for some intelligent system, such as robot and unmanned vehicle, which need the precise location services. The average localization error of the proposed placement scheme can be reduced by 28.2% and 12.5% compared to the random scheme and the default DE-based scheme. In addition, an indoor navigation effectiveness of 92% was achieved.

Similar to the fingerprinting localization, the multilateration localization requires pre-configuration tool, which is one of the main disadvantages of this method, while the number of anchors increases. For a larger area, more anchors are required to provide enough LOS measurements in the proposed method. Future work will include the exploration and improvement of anchor placement scheme to increase the indoor localization accuracy even more.

Table 7 Summary of related work in comparison with the method proposed in this paper

Method	Technology	Environment	Evaluation
Segura et al. [26]	UWB	Room (6 m × 8 m)	Error 0.2 m
Gropwindhager et al. [10]	UWB	Office room (4 m × 6 m)	Error 0.2 m
Tian et al. [30]	WiFi fingerprint, Coverage-CRLB placement	Floor (29 m × 14 m)	Improve 31%
Chen et al. [6]	WiFi fingerprint, Coverage-MFD placement	Floor (29 m × 14 m)	Improve 16%
Wang et al. [34]	UWB, GA placement	L shape area (8.3 m × 1.6 m)	Error 0.16 m
AL-Madani et al. [1]	BLE fingerprint, fuzzy logic	Floor (52.5 m × 12.5 m)	Error 0.43 m
Proposed	UWB, CRLB-DE placement	Floor (31 m × 28.5 m)	Improve 28.2%

Acknowledgements This work was supported by the National Natural Science Foundation of China (Grants No. 61877067), Key Laboratory Foundation for Near Ground Detection and Perception technology (TCGZ2019A002, TCGZ2020E00511, 6142414200511) and Foundation of Basic research projects (61424140502).

Declarations

Conflict of interest The authors declare that they have no conflict of interest.

References

1. AL-Madani B, Orujov F, Maskeliūnas R, Damaševičius R, Venčkauskas A (2019) Fuzzy logic type-2 based wireless indoor localization system for navigation of visually impaired people in buildings. Sensors. https://doi.org/10.3390/s19092114
2. Alia OM, Al-Ajouri A (2017) Maximizing wireless sensor network coverage with minimum cost using harmony search algorithm. IEEE Sens J 17(3):882–896. https://doi.org/10.1109/JSEN.2016.2633409
3. Alipio MI, Peñalosa KMT, Unida JRC (2020) In-store customer traffic and path monitoring in small-scale supermarket using UWB-based localization and SSD-based detection. J Ambient Intell Humaniz Comput. https://doi.org/10.1007/s12652-020-02236-z
4. Alsmady A, Awad F (2017) Optimal Wi-Fi access point placement for RSSI-based indoor localization using genetic algorithm. In: 2017 8th international conference on information and communication systems (ICICS), pp 287–291. https://doi.org/10.1109/IACS.2017.7921986
5. Bhatti MA, Riaz R, Rizvi SS, Shokat S, Riaz F, Kwon SJ (2020) Outlier detection in indoor localization and internet of things (IOT) using machine learning. J Commun Netw 22(3):236–243. https://doi.org/10.1109/JCN.2020.000018
6. Chen Q, Wang B, Deng X, Mo Y, Yang LT (2013) Placement of access points for indoor wireless coverage and fingerprint-based localization. In: 2013 IEEE 10th international conference on high performance computing and communications 2013 IEEE international conference on embedded and ubiquitous computing, pp 2253–2257. https://doi.org/10.1109/HPCC.and.EUC.2013.323
7. Deif DS, Gadallah Y (2017) An ant colony optimization approach for the deployment of reliable wireless sensor networks. IEEE Access 5:10744–10756. https://doi.org/10.1109/ACCESS.2017.2711484
8. DoğançSay K, Hmam H (2008) Optimal angular sensor separation for AOA localization. Signal Process 88(5):1248–1260. https://doi.org/10.1016/j.sigpro.2007.11.013
9. Eldeeb H, Arafa M, Faheem Saidahmed MT (2017) Optimal placement of access points for indoor positioning using a genetic algorithm. In: 2017 12th international conference on computer engineering and systems (ICCES), pp 306–313. https://doi.org/10.1109/ICCES.2017.8275323
10. Growindhager B, Rath M, Kulmer J, Hinteregger S, Rmer K (2017) Demo abstract: Uwb-based single-anchor low-cost indoor localization system. In: SenSys '17
11. He G, Yuan X, Zhuang Y, Hu H (2020) An integrated GNSS/LIDAR-SLAM pose estimation framework for large-scale map building in partially GNSS-denied environments. IEEE Trans Instrum Meas. https://doi.org/10.1109/TIM.2020.3024405
12. Hosseinzadeh S, Larijani H, Curtis K, Wixted A, Amini A (2017) Empirical propagation performance evaluation of LORA for indoor environment. In: 2017 IEEE 15th international conference on industrial informatics (INDIN), pp 26–31. https://doi.org/10.1109/INDIN.2017.8104741
13. Jie H, Liu K, Zhang H, Xie R, Wu W, Guo S (2020) AODC: automatic offline database construction for indoor localization in a hybrid UWB/Wi-Fi environment. In: 2020 IEEE/CIC international conference on communications in China (ICCC), pp 324–329. https://doi.org/10.1109/ICCC49849.2020.9238772
14. Jin F, Liu K, Zhang H, Ng JK, Guo S, Lee VCS, Son SH (2020) Toward scalable and robust indoor tracking: design, implementation, and evaluation. IEEE Internet Things J 7(2):1192–1204. https://doi.org/10.1109/JIOT.2019.2953376
15. Kar K, Datta S, Pal M, Ghatak R (2016) Motley Keenan model of in-building coverage analysis of IEEE 802.11N WLAN signal in electronics and communication engineering department of national institute of technology Durgapur. In: 2016 international conference on microelectronics, computing and communications (MicroCom), pp 1–6. https://doi.org/10.1109/MicroCom.2016.7522577
16. Khezri S, Faez K, Osmani A (2010) Modified discrete binary PSO based sensor placement in WSN networks. In: 2010 international conference on computational intelligence and communication networks, pp 200–204. https://doi.org/10.1109/CICN.2010.49
17. Lei P, Huang X, Wang J, Ma X (2012) Sensor placement of multistatic radar system by using genetic algorithm. In: 2012 IEEE international geoscience and remote sensing symposium, pp 4782–4785. https://doi.org/10.1109/IGARSS.2012.6352544
18. Lei WB (2009) Station arrangement strategy of TDOA/AOA location system based on genetic algorithm. Comput Eng Appl 45(24):219. https://doi.org/10.3778/j.issn.1002-8331.2009.24.066
19. Liang J, Liu D (2010) Joint elevation and azimuth direction finding using l-shaped array. IEEE Trans Antennas Propag 58(6):2136–2141. https://doi.org/10.1109/TAP.2010.2046838
20. Liang J, Zhang T, Yang Y, Cui G, Kong L, Yang X, Yang J (2016) Preferential optimal antenna placement for mimo radar under the situation of multiple surveillance regions. In: 2016 CIE international conference on radar (RADAR), pp 1–4. https://doi.org/10.1109/RADAR.2016.8059151
21. Liu K, Zhang H, Ng JK, Xia Y, Feng L, Lee VCS, Son SH (2018) Toward low-overhead fingerprint-based indoor localization via transfer learning: design, implementation, and evaluation. IEEE Trans Ind Inf 14(3):898–908. https://doi.org/10.1109/TII.2017.2750240
22. Orujov F, Maskeliūnas R, Damaševičius R, Wei W, Li Y (2018) Smartphone based intelligent indoor positioning using fuzzy logic. Future Gener Comput Syst 89:335–348. https://doi.org/10.1016/j.future.2018.06.030
23. Rajagopal N, Chayapathy S, Sinopoli B, Rowe A (2016) Beacon placement for range-based indoor localization. In: 2016 international conference on indoor positioning and indoor navigation (IPIN), pp 1–8. https://doi.org/10.1109/IPIN.2016.7743626
24. Rao X, Li Z (2019) MSDFL: a robust minimal hardware low-cost device-free WLAN localization system. Neural Comput Appl 31(12):9261–9278. https://doi.org/10.1007/s00521-018-3945-8
25. Sadhukhan P, Dahal K, Pervez Z (2017) Impact of beacon coverage on clustering strategies for fingerprinting localization system. In: 2017 international conference on computing, networking and communications (ICNC), pp 184–188. https://doi.org/10.1109/ICCNC.2017.7876124
26. Segura M, Mut V, Sisterna C (2012) Ultra wideband indoor navigation system. IET Radar Sonar Navig 6(5):402–411
27. Sharma C, Wong YF, Soh W, Wong W (2010) Access point placement for fingerprint-based localization. In: 2010 IEEE international conference on communication systems, pp 238–243. https://doi.org/10.1109/ICCS.2010.5686092

28. Tao Q, Cao Y, Yimwadsana B, Fu X (2020) RSS-based underwater acoustic distance measurement with multiple frequencies. Ocean Eng 215:107772. https://doi.org/10.1016/j.oceaneng.2020.107772
29. Tekdas O, Isler V (2010) Sensor placement for triangulation-based localization. IEEE Trans Autom Sci Eng 7(3):681–685. https://doi.org/10.1109/TASE.2009.2037135
30. Tian Y, Huang B, Jia B, Zhao L (2020) Optimizing AP and beacon placement in WiFi and BLE hybrid localization. J Netw Comput Appl 164:102673. https://doi.org/10.1016/j.jnca.2020.102673
31. Tiemann J, Schweikowski F, Wietfeld C (2015) Design of an UWB indoor-positioning system for UAV navigation in GNSS-denied environments. In: 2015 international conference on indoor positioning and indoor navigation (IPIN), pp 1–7. https://doi.org/10.1109/IPIN.2015.7346960
32. Tolza X, Acco P, Fourniols JY, Soto-Romero G, Escriba C, Bracq M (2019) Optimal uncalibrated RSS indoor positioning and optimal reference node placement using Cramér–Rao lower bound. J Sens 2019:5494901. https://doi.org/10.1155/2019/5494901
33. Vedadi F, Valaee S (2020) Automatic visual fingerprinting for indoor image-based localization applications. IEEE Trans Syst Man Cybern: Syst 50(1):305–317. https://doi.org/10.1109/TSMC.2017.2695080
34. Wang S, Wang S, Liu W, Tian Y (2020) A study on the optimization nodes arrangement in UWB localization. Measurement 163:108056. https://doi.org/10.1016/j.measurement.2020.108056
35. Wang W, Bai P, Li H, Liang X (2018) Optimal configuration and path planning for UAV swarms using a novel localization approach. Appl Sci 8(6):1001
36. Wang X, Wang Z, O'Dea B (2003) A TOA-based location algorithm reducing the errors due to non-line-of-sight (NLOS) propagation. IEEE Trans Veh Technol 52(1):112–116. https://doi.org/10.1109/TVT.2002.807158
37. He Y, Meng W, Ma L, Deng Z (2011) Rapid deployment of aps in WLAN indoor positioning system. In: 2011 6th international ICST conference on communications and networking in China (CHINACOM), pp 268–273. https://doi.org/10.1109/ChinaCom.2011.6158161
38. Lin Y, Zhang G (2003) The optimal arrangement of four laser tracking interferometers in 3d coordinate measuring system based on multi-lateration. In: IEEE international symposium on virtual environments, human–computer interfaces and measurement systems, 2003. VECIMS '03. 2003, pp 138–143. https://doi.org/10.1109/VECIMS.2003.1227044
39. Zhang H, Liu K, Jin F, Feng L, Lee V, Ng J (2020) A scalable indoor localization algorithm based on distance fitting and fingerprint mapping in Wi-Fi environments. Neural Comput Appl 32(9):5131–5145. https://doi.org/10.1007/s00521-018-3961-8
40. Zhao Y, Zhou H, Li M (2008) Indoor access points location optimization using differential evolution. In: 2008 international conference on computer science and software engineering, vol 1, pp 382–385. https://doi.org/10.1109/CSSE.2008.1539
41. Zirazi S, Canalda P, Mabed H, Spies F (2012) Wi-fi access point placement within stand-alone, hybrid and combined wireless positioning systems. In: 2012 fourth international conference on communications and electronics (ICCE), pp 279–284. https://doi.org/10.1109/CCE.2012.6315912